

1 A Fast Method for Detecting Rock Blocks and Calculating Volumes 2 and 3D Surface Areas

3 Ali Polat

4 Provincial Directorate of Disaster and Emergency, 58000, Sivas, Turkey

5 ARTICLE INFO

6
7 **Keywords:**
8 Convolutional Neural Networks
9 3D Surface Area Calculation
10 Volume Calculation
11 Rock segmentation
12 Rockfall
13 U-Net

ABSTRACT

14 Rockfall events are a type of natural disaster that causes loss of life and property in the world.
15 The risk of rockfall can be eliminated by using rockfall prevention methods. To choose the most
16 suitable method, projecting studies should be carried out. This study aims to automatically detect
17 rock blocks in a region and calculate their volumes and 3D surface areas. For this purpose, U-Net
18 segmentation method and Python software language were used. DenseNet121 transfer learning
19 method based on convolutional neural networks was used for feature extraction. The data set
20 was created from the orthophoto images obtained by an unmanned aerial vehicle (UAV). Using
21 the random sampling method, 369 images were selected for training and 191 images for test. As
22 a result of the analysis, the IOU (Intersection Over Union) was calculated as 85% for training
23 and 84% for test. The trained model was applied to the study area and 3111 rock blocks were
24 detected. The resulting map is saved as a vector file with coordinates and can be opened in any
25 GIS software. The volumes and 3D surface areas of the rock blocks were calculated with Python
26 script as 275.93 m^3 and 2615.23 m^2 , respectively. With this study, rock blocks can be detected
of objects.

27

28 1. Introduction

29 In many parts of the world, loss of life and property is experienced, and large-scale economic losses occur due to
30 natural disasters. One of these natural disasters is rockfall events. Rockfalls are a type of slope instability in which
31 blocks of rock confined to discontinuities move very rapidly from the source region (Varnes, 1978; Hutchinson, 1988;
32 Cruden and Varnes, 1996). Due to the high velocity during the event, rockfalls can be very dangerous for structures in
33 their route depending on the block size. Although it is a type of disaster that affects small areas, its consequences can
34 be very serious. That's why rockfall prevention studies are important. There are studies on this subject in the literature
35 (Liu et al., 2021; Keskin and Polat, 2022; Ji et al., 2023; Kainthola et al., 2023; Cao et al., 2024). Some preliminary
36 studies are needed to develop a prevention method. One of them is the detection of rock blocks and the calculation of
37 their geometric properties. In this study, rock blocks were segmented, and their volumes and 3D surface areas were
38 calculated.

39 There are various studies on rock segmentation in the literature. Dunlop (2006) developed a technique for the
40 characterization of rocks using albedo, color, texture, and shape features. In that work, rocks in natural scenes were
41 accurately segmented and localized with precise boundaries. The authors successfully combined top-down and bottom-

ORCID(s): 0000-0002-9147-3633 (A. Polat)

42 up knowledge for segmentation and performed geologic rock analysis effectively.

43 In a study conducted by Song and Shan (2006), rock segmentation techniques were applied to Martian images with
44 the aim of planning routes and identifying potential landing areas. The researchers developed texture-based image seg-
45 mentation methods that utilize edge-flow driven active contours. They also combined wavelet-based local transforms,
46 multi-resolution histograms, and inter-scale decision strategies for more effective rock segmentation. Through their
47 experiments, Song and Shan (2006) successfully obtained reliable rock segmentation results.

48 The place of visual navigation in planetary rover autonomy is crucial. Rock segmentation is an important and
49 challenging task for rover autonomy due to the high computational load and real-time requirement. Kuang et al.
50 (2021) propose a rock segmentation network (NI-U-Net++) to aid in the visual navigation of rovers. The created
51 model consists of two steps. In the first step, called pre-training, synthetic rock images are generated and used to
52 pre-train the NI-U-Net++ network. In the second phase, transfer-training, the pre-trained NI-U-Net++ network is
53 fine-tuned using real-life images.

54 Guo et al. (2022) proposed an adaptive watershed segmentation method based on distance transformation for blasted
55 rock piles images. They obtained 95.65% segmentation accuracy for limestone and granite rock blocks with area over
56 100 cm².

57 Segmentation of rocks is important in mining as well as in geology. Segmentation is used in this area to determine
58 the size distribution of rock fragments, to organize and optimize blasting, and to reduce environmental impact. For this
59 purpose, Malladi et al. (2014) proposed a simple superpixel algorithm called Superpixels Using Morphology (SUM),
60 which uses a watershed transformation approach to generate superpixels; and made a study comparing some of the
61 current superpixel algorithms on rock images.

62 Recently, various deep learning and machine learning algorithms, including Convolutional Neural Networks (CNN),
63 have been proposed by researchers working on rock segmentation. Karimpouli and Tahmasebi (2019) used convolu-
64 tional autoencoder networks called SegNet for segmentation of digital rock images. Due to the limited number of rock
65 images, cross-correlation based simulation was applied to increase the number of images. 20 images taken from Berea
66 sandstone were used as dataset. As a result of the experiments, they obtained an accuracy value of 96%.

67 Xue et al. (2021) made rock segmentation study for a different purpose; they proposed the rock segmentation
68 visual system to assist Tunnel Boring Machine (TBM) driving. TBM is an essential equipment for digging long-range
69 tunnels. They applied different deep learning network for semantic segmentation of rocks.

70 In the above studies, rock segmentation was carried out for different purposes. In this study, rock segmentation
71 was carried out as a necessary preliminary study in the development of rockfall prevention methods. Rock blocks
72 were detected precisely in a fast, economical, and safe manner. In addition, the volumes and 3D surface areas of rock
73 blocks were calculated. The methods and algorithms used in the study can be used in many fields such as engineering

74 applications, and geological-geomorphological studies.

75 **1.1. Study area**

76 The study area is in the north of Karasar village, which is approximately 156 km away from Sivas city (Fig. 1).
 77 This area consists of Middle Miocene aged agglomerate and tuff units (MTA 1/25000) (Fig. 2). This unit was defined
 78 as Adatepe volcanites according to Yilmaz and Yilmaz (2004). The unit consists of black, red-brown, and brown-
 79 black colored basaltic lava flows and less commonly agglomerate and tuffs. The rock blocks in this unit expose a risk
 80 of rockfall. Lower Miocene aged sandstone-mudstone-limestone units are observed in the settlement area (Karasar
 81 village) and vicinity.

82 Karasar village is located on the slopes of a hill. The bedrock on the hill is heavily fractured and cracked. There are
 83 many rock blocks that have fallen from the upper parts of the slope. The sizes of these blocks vary from 0.5 m³ to 15
 84 m³. Rapid temperature changes, heavy snow and precipitation, freeze-thaw cycles, earthquakes, and human-induced
 85 factors increase the risk of rockfall in the region.

86 **2. Methodology**

87 Creating the dataset is a big problem for classification or segmentation processes. In this study, Unmanned Air
 88 Vehicle (UAV) was used to collect data. An orthophoto image of the region was created from aerial photographs
 89 obtained by UAV. Model building processes were conducted in a part of the study area. Training and testing images
 90 were generated from this region. Rock blocks were labeled, and mask images were created. The segmentation process
 91 was then carried out using Python and necessary libraries, and the results were converted into polygon vector files.
 92 Additionally, the volumes and 3D surface areas of all the rocks were calculated (Fig. 3).

93 **2.1. Data preparation**

94 In this study required data was collected by UAV. DJI phantom 3-Pro was used for image acquisition. First, the
 95 area to be flown is determined, then the necessary parameters for image acquisition are entered by the Pix4d Capture
 96 software. These parameters were chosen as follows.

- 97 – Flight altitude (altitude): 100 m.
 98 – Flight speed (speed): Fast
 99 – Camera angle (Angle): 70°
 100 – Overlap: 80%

101

102 The flight was carried out by the "Double Grid" method. The model of UAV used in this study does not have an
 103 obstacle detecting feature. Therefore, when determining the height, it is necessary to pay attention to the nearby power

104 lines, tall buildings, trees, and peaks of hills.

105 The camera model (FC00X) of UAV has 4000×3000 resolution, 3.61 mm focal length and 1.56×1.56 μm pixel
 106 dimensions. After the flight, 284 images were obtained, and these images were processed with the Pix4Dmapper
 107 software. As a result, an orthophoto image with a resolution of 3.51 cm/pixel and a dimension of 2329×1587 was
 108 created.

109 A region was selected from a large orthophoto image to create training and testing images. This area was chosen
 110 randomly. All visible rocks in the image were outlined using GIS software. The resulting file was saved as a vector
 111 file and used as mask data in the segmentation process. Following this, image and mask files were created separately.

112 A deep learning model requires the same-sized images. That's why a single image needs to be split into patches.
 113 The patch dimension was used as 256×256. Train-test splitting rate was selected as 66% for training data and 34% for
 114 testing data. The large image was split into 9 parts to avoid sampling from the same regions. Areas 1,5, and 9 were
 115 selected for creating test images. Train images were selected from the other (2,3,4,6,7,8) areas (Fig. 4). A total of
 116 560 images (256×256) were selected, 369 images for training and 191 images for testing. The same processes were
 117 applied to extract the mask images.

118 The Albumentations (Buslaev et al., 2020) method was also used for data augmentation during the model-building
 119 stage. Albumentations includes many transform methods. The augmentation methods listed below were applied:

- 120 – horizontal flip
- 121 – affine transforms
- 122 – perspective transforms
- 123 – brightness/contrast/colours manipulations
- 124 – image blurring and sharpening
- 125 – gaussian noise

126

127 **2.2. Model building**

128 In this study, U-Net architecture (Ronneberger et al., 2015) was used as segmentation model. This architecture is
 129 a type of fully convolutional network developed for biomedical image segmentation. It is named U-Net because the
 130 shape of the architecture is like the letter U. The network architecture of U-Net is shown in Fig. 5. It consists of two
 131 parts: contracting path (left side) and expanding path (right side). The first part captures context, and the second part
 132 enables precise localization. The left side consists of four blocks and each block contains two 3×3 convolution layers
 133 + activation function (with batch normalization) and one 2×2 max-pooling layer. Also, the right side consists of four
 134 blocks. These blocks include the steps of deconvolution layer, merging with feature map from subsampling path, 3×3

135 convolution layer + activation function (with batch normalization). Finally, an additional 1×1 convolution operation
 136 is applied to reduce the feature map to the required number of channels and generate the segmented image.

137 DenseNet121 transfer learning model was used for feature extraction and rock segmentation was performed with
 138 U-Net. Segmentation model was evaluated in terms of IoU and F1-score metrics. IoU, which is frequently preferred in
 139 segmentation problems, is also known as the Jaccard similarity coefficient (Jaccard, 1912). It is the ratio of correctly
 140 classified pixels to the sum of the number of pixels in that class and the predicted number of pixels (Equation 1).

$$J(A, B) = \frac{|A \cap B|}{|A \cup B|} \quad (1)$$

141 The F1-Score is important in that it is not False Negative or False Positive, but a measurement metric that includes all
 142 error costs. It is the harmonic mean of Precision and Recall values (Equation 2).

$$F1\text{-}Score = \frac{2 \times \text{Precision} \times \text{Recall}}{\text{Precision} + \text{Recall}} \quad (2)$$

$$\text{Precision} = \frac{TP}{TP + FP} \quad (3)$$

$$\text{Recall} = \frac{TP}{TP + FN} \quad (4)$$

143 Where TP is True Positive, FP is False Positive and FN is False Negative.

144 3. Results

145 In this study, we created our own dataset. A large orthophoto image with a dimension of 2329×1587 was created
 146 from UAV images. This image needs to be patched for use in the segmentation model. A python script has been written
 147 for this purpose. It is possible to create the desired number and size of images with the written script. Random corner
 148 coordinates with the size of 256×256 patches were created. Obtaining images with the exact corner coordinates was
 149 prevented. Because of this condition, the program gives an error when too many images are wanted to be created.
 150 Also, the probability of creating very similar images increases. Using the grid method, 56 images can be obtained

Table 1
Model parameters

Optimizer	Adam
Learning rate	0.0001
Batch size	8
Image size	256×256
Epoch	100

151 from the large orthophoto image. Using the random sampling method 560 images were obtained from the same image.
 152 U-Net segmentation model was used with DenseNet121. IOU and F1-score were used as performance metrics.
 153 The model was trained and tested with different parameters. The parameters providing the best results are given in
 154 Table 1 below.

155 IoU scores and losses graph of model are shown in Figure 6. The results of the model are satisfactory for the
 156 segmentation task. Train IoU, test IoU, train F1-score and test F1-score were calculated as 0.85%, 0.85%, 0.92%, and
 157 0.92%, respectively.

158 The trained model successfully detected rock blocks within the study area (Fig. 7). The boundaries of 3111 rocks
 159 of various sizes were determined and created as a vector file (.shp). This detection method is not recommended for
 160 smaller areas. Because sufficient training data cannot be created. In areas where there are several rock blocks, detection
 161 can also be done manually. Sometimes there may be distortions at the edges and corners of the image. This causes
 162 errors in rock block detection. Therefore, a larger area than the area where the rocks are located should be selected as
 163 the study area.

164 After the rocks were detected, each rock's volume and 3D surface area were calculated. These calculations were
 165 performed using Python. Calculated values were saved in the shape file as fill volume, cut volume and 3D area.

166 In volume calculations, there must be a reference height or surface. In this study, the heights at the boundaries of
 167 the rocks were selected as the reference height. The calculations were made using an image containing elevation data.
 168 This image consists of pixels containing elevation values, which are organized into rows and columns. The elevation
 169 values in each row were used to calculate the total volume. The polygons showing the boundaries of the rocks were
 170 masked with elevation data. Thus, data with elevation values for each rock were obtained. Volumes were calculated
 171 by proceeding along the rows. The slope was calculated by comparing the elevation values at the beginning and end
 172 of the row. A new base elevation was determined for each pixel and the volumes were calculated from this elevation.

173 In this method, it is necessary to evaluate three different scenarios. In the first case, the first and last elevations of
 174 the rows are equal. Here, the starting elevation value is used as the reference height. Volumes above this elevation are
 175 calculated as fill volumes, while volumes below are calculated as cut volumes. In the second case, the first elevation
 176 is greater than the last elevation of the rows. In the third case, the first elevation is less than the last elevation of the

177 rows. Different calculations are required for each scenario. These situations are illustrated in Figure 8.

178 Volume calculation can be easily done by multiplying the pixel area by the height. Heights need to be calculated
 179 for each pixel. The starting and ending pixels along a row are assumed to be ground. These ground elevations are used
 180 to find the slope, and each pixel's height is recalculated using this slope. Fill volume and cut volume were calculated
 181 using new heights and pixel areas. Slopes, fill volumes and cut volumes were determined using the method in Figure
 182 8. The total volumes (fill and cut) are found by summing the calculations made for each row.

183 The 3D surface area was calculated by Python script. Calculations of flat surfaces can be found by multiplying
 184 pixel lengths. However, different methods must be used for irregular surfaces. The gradient method was used in 3D
 185 surface calculation. Height changes were calculated in X and Y directions, gradient vectors were obtained in each
 186 direction. Surface areas were calculated by using these vectors. The slope correction equation is used to determine the
 187 sloped surfaces (Equation 5).

$$\text{slope correction} = \sqrt{1 + \left(\frac{\partial z}{\partial x}\right)^2 + \left(\frac{\partial z}{\partial y}\right)^2} \quad (5)$$

$$\frac{\partial z}{\partial x} = \text{gradient in X direction}, \quad \frac{\partial z}{\partial y} = \text{gradient in Y direction} \quad (6)$$

188 The 3D surface area is calculated as following:

$$\text{3D surface area} = \sum \text{pixel area} \times \text{slope correction} \quad (7)$$

189 4. Conclusions

190 This study aims to segment rock blocks and calculate the volume and 3D surface areas of the blocks obtained as a
 191 result of segmentation. The methods used in the segmentation process provided the determination of the boundaries
 192 of rock blocks with high accuracy rates. In this way, the geometric properties of the blocks were analysed in detail.

193 U-Net deep learning network and DenseNet121 model were used as segmentation methods. The boundaries of
 194 rock blocks were determined accurately with the trained model.

195 The volume of each rock block was successfully calculated from the data obtained after segmentation. Similarly,
 196 the 3D surface areas of the blocks were calculated. High-resolution Digital Elevation Map (DEM) data were used in
 197 volume and surface area calculations. Determination of block volumes and 3D surface areas is of critical importance,

198 especially for rockfall simulations and engineering analyses. In addition, since the outputs of the study are coordinated
199 vector data, they can be easily used in any GIS software. It can be a basis for different studies and analyses.

200 This study has presented a reliable method for segmentation and volume/surface area calculations and has also
201 directly contributed to engineering applications in terms of determining the physical properties of rock masses. The
202 segmentation section of the study is recommended for terrains containing a lot of rock blocks. It is possible to detect
203 rock blocks in a short time. In addition, this method can be used to automatically detect different types of terrain. This
204 study requires DEM and orthophoto images obtained from the field. A region is selected and labelled objects in any
205 GIS software for training the model. The following processes are carried out entirely with Python scripts.

206 Deep learning models usually require a large amount of data for training. A large amount of data can be generated
207 with the Random Sampling method proposed in this study. Volume and 3D surface area algorithms can be used not
208 only for rock blocks but also for any object on the field. These algorithms only require precise DEM data and object
209 boundaries. For example, these calculations can be made for a single rock block. In these calculations, ground heights
210 and object heights must be determined clearly. When determining the object boundaries, they should be extended
211 towards the ground. If the boundaries only represent the object, the ground heights will not be considered, and the
212 results will not be correct. In some cases, the model can draw the boundaries of the rock blocks narrower. In this case,
213 this problem can be solved by adding buffers to the rock blocks.

214 As a result, this study provides a basis for volumetric and geometric analyses for rock mechanics, geology and
215 engineering applications, and can be expanded by testing on different rock types and fields in future studies.

216 5. Acknowledgments

217 The author wants to thank the Prime Ministry Disaster and Emergency Management Authority for supplying or-
218 thophoto images and geological map.

219 **Code availability section**

220 Name of the code: rock_segmentation

221 Contact: ali.polat@afad.gov.tr

222 Program language: Python

223 Software required: Python v3.9

224 Program size: 35.7 KB

225 The source codes are available for downloading at the link: https://github.com/apolat2018/rock_segmentation226 **References**

- 227 Buslaev, A., Iglovikov, V.I., Khvedchenya, E., Parinov, A., Druzhinin, M., Kalinin, A.A., 2020. Albumentations: fast and flexible image augmen-
228 tations. *Information* 11, 125.
- 229 Cao, Z., Liu, Z., Xu, G., Lin, H., Li, X., Nikitas, N., 2024. Risk assessment and prevention for typical railway bridge pier under rockfall impact, in:
230 *Structures*, Elsevier. p. 106178.
- 231 Cruden, D.M., Varnes, D.J., 1996. Landslide types and processes. *Transportation Research Board, US National Academy of Sciences, Special*
232 *Report 247*, 36–75.
- 233 Dunlop, H., 2006. Automatic rock detection and classification in natural scenes. *Masters Thesis, Carnegie Mellon University* .
- 234 Guo, Q., Wang, Y., Yang, S., Xiang, Z., 2022. A method of blasted rock image segmentation based on improved watershed algorithm. *Scientific*
235 *Reports* 12, 7143.
- 236 Hutchinson, J., 1988. Morphological and geotechnical parameters of landslides in relation to geology and hydrogeology, landslides, in: *Proceedings*
237 *of the fifth international symposium on landslides*, pp. 3–35.
- 238 Jaccard, P., 1912. The distribution of the flora in the alpine zone. 1. *New phytologist* 11, 37–50.
- 239 Ji, Z.M., Chen, T.L., Wu, F.Q., Li, Z.H., Niu, Q.H., Wang, K.Y., 2023. Assessment and prevention on the potential rockfall hazard of high-steep
240 rock slope: a case study of zhongyuntai mountain in lianyungang, china. *Natural Hazards* 115, 2117–2139.
- 241 Kainthola, A., Pandey, V.H.R., Singh, P., Singh, T., 2023. Stability assessment of markundi hills using q-slope, smr and simulation tools, in:
242 *Landslides: Detection, Prediction and Monitoring: Technological Developments*. Springer, pp. 87–107.
- 243 Karimpouli, S., Tahmasebi, P., 2019. Segmentation of digital rock images using deep convolutional autoencoder networks. *Computers & geosciences*
244 126, 142–150.
- 245 Keskin, İ., Polat, A., 2022. Kinematic analysis and rockfall assessment of rock slope at the unesco world heritage city (safranbolu/turkey). *Iranian*
246 *Journal of Science and Technology, Transactions of Civil Engineering* 46, 367–384.
- 247 Kuang, B., Wisniewski, M., Rana, Z.A., Zhao, Y., 2021. Rock segmentation in the navigation vision of the planetary rovers. *Mathematics* 9, 3048.
- 248 Liu, W.l., Dong, J.x., Xu, H.h., Sui, S.g., Yang, R.x., Zhou, L.s., 2021. Trajectory analysis and risk evaluation of dangerous rock mass instability of
249 an overhang slope, southwest of china. *Advances in civil engineering* 2021, 7153535.
- 250 Malladi, S.R.S., Ram, S., Rodríguez, J.J., 2014. Superpixels using morphology for rock image segmentation, in: *2014 Southwest Symposium on*
251 *Image Analysis and Interpretation*, IEEE. pp. 145–148.
- 252 Ronneberger, O., Fischer, P., Brox, T., 2015. U-net: Convolutional networks for biomedical image segmentation, in: *Medical image computing and*
253 *computer-assisted intervention–MICCAI 2015: 18th international conference, Munich, Germany, October 5–9, 2015, proceedings, part III* 18,
254 *Springer*. pp. 234–241.

Short title

- 255 Song, Y., Shan, J., 2006. A framework for automated rock segmentation of the mars exploration rover imagery. URL: <https://api.semanticscholar.org/CorpusID:39798752>.
- 256
- 257 Varnes, D., 1978. Slope movement types and processes. *Landslides: analysis and control* .
- 258 Xue, Z., Chen, L., Liu, Z., Lin, F., Mao, W., 2021. Rock segmentation visual system for assisting driving in tbm construction. *Machine Vision and*
- 259 *Applications* 32, 77.
- 260 Yılmaz, H., Yılmaz, A., 2004. Divriği (sivas) yöresinin jeolojisi ve yapısal evrimi. *Türkiye Jeoloji Bülteni* 47, 13–46.

261 **List of Figures**

262 1	Location map	12
263 2	Geological map (1/25000 scale geological map of General Directorate of Mineral Research and Ex-	13
264 plorations) (a), rock blocks (b), settlement and rocks (c)		
265 3	Workflow diagram	14
266 4	Train and test sampling areas. 1,5,9 test sampling area and 2,3,4,6,7,8 train sampling area	15
267 5	U-Net architecture	16
268 6	DenseNet121 IoU and Loss values	17
269 7	Result map of the model (a) original view, (b,c,d)zoomed views.	18
270 8	Volume calculation methods. (a) first height is greater than the last height of the rows,(b) b) first height	
271 is less than the last height of the rows	19	

Short title

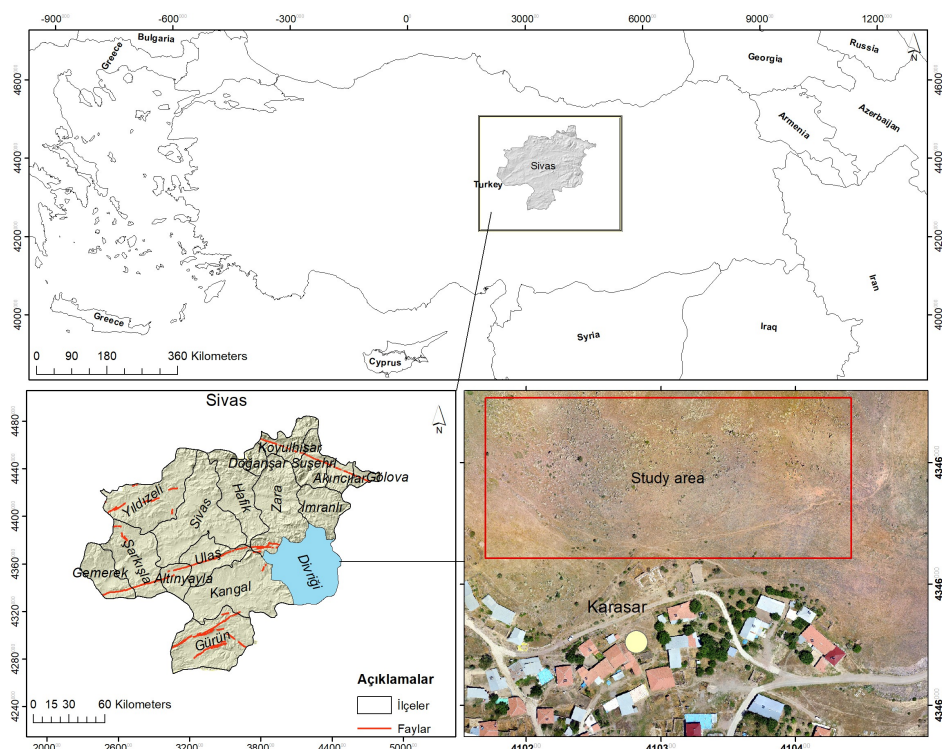
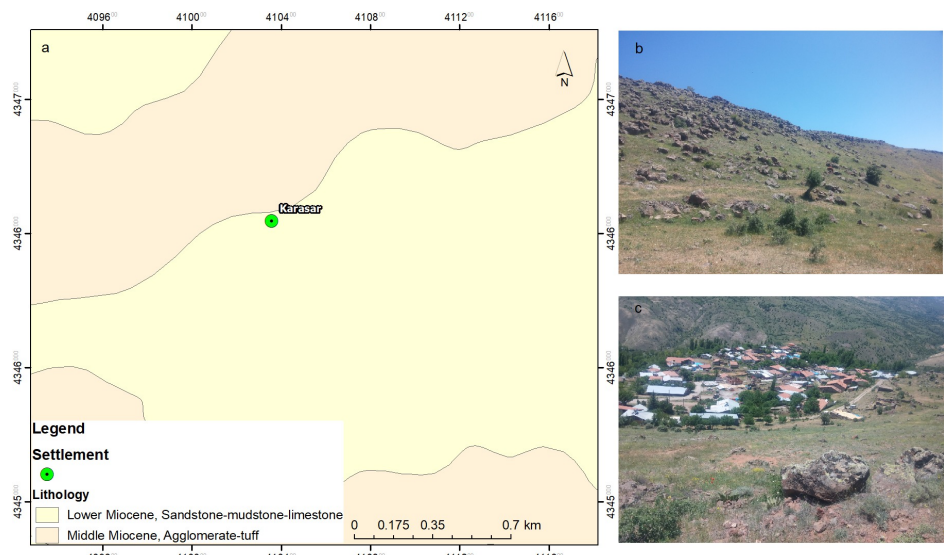


Figure 1: Location map



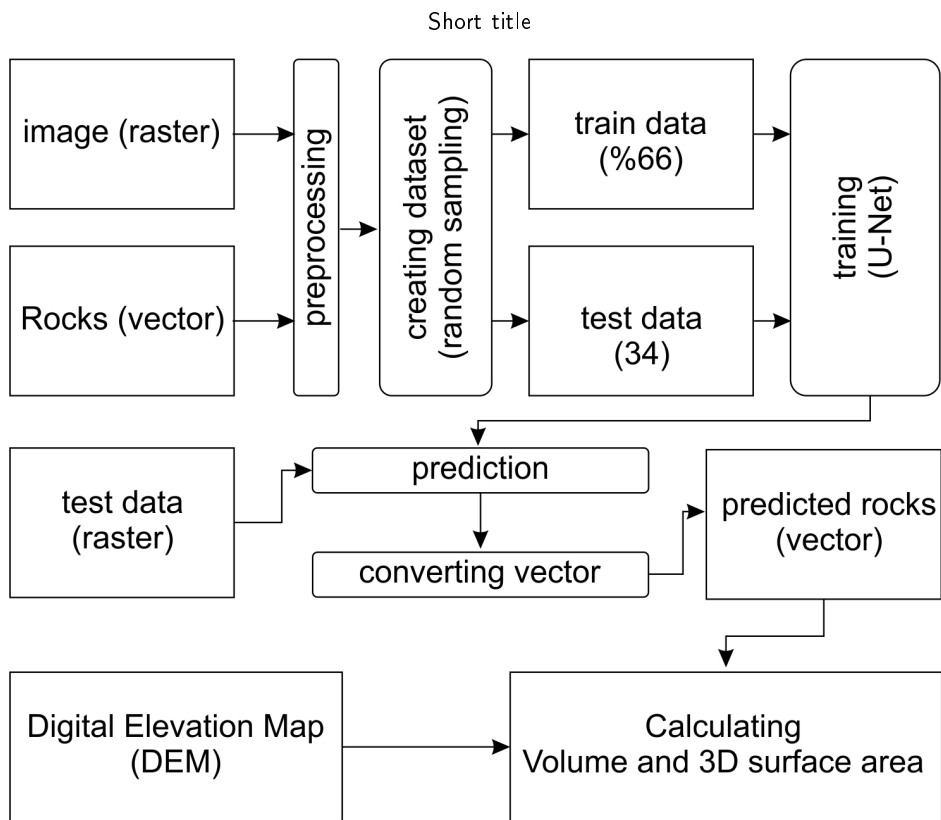


Figure 3: Workflow diagram

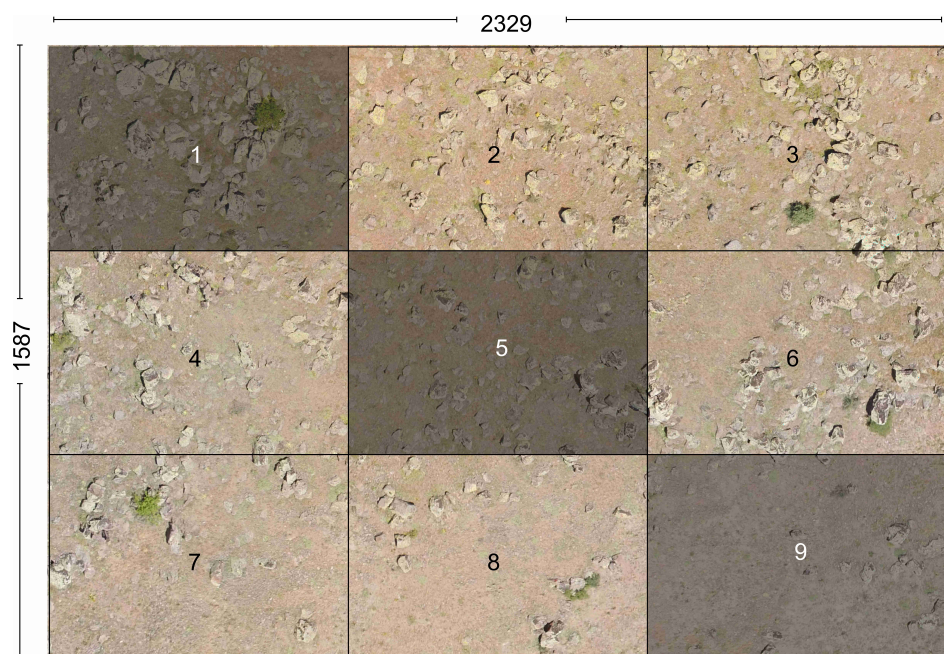


Figure 4: Train and test sampling areas. 1,5,9 test sampling area and 2,3,4,6,7,8 train sampling area

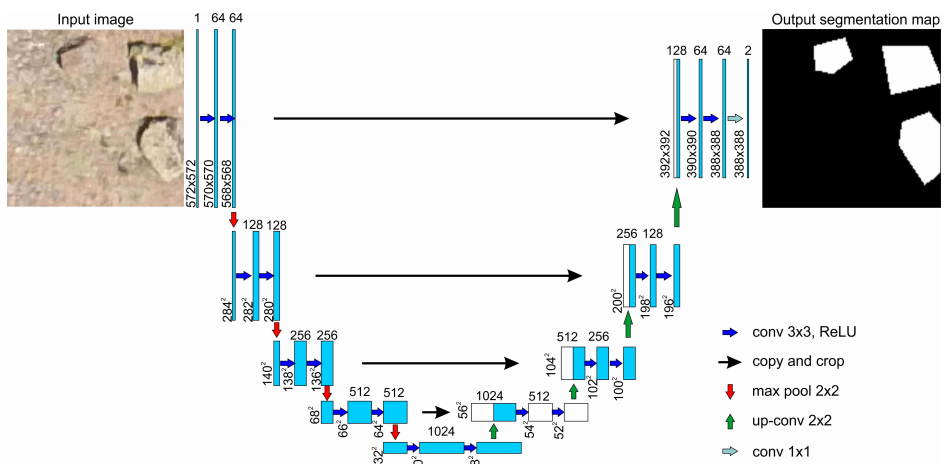


Figure 5: U-Net architecture

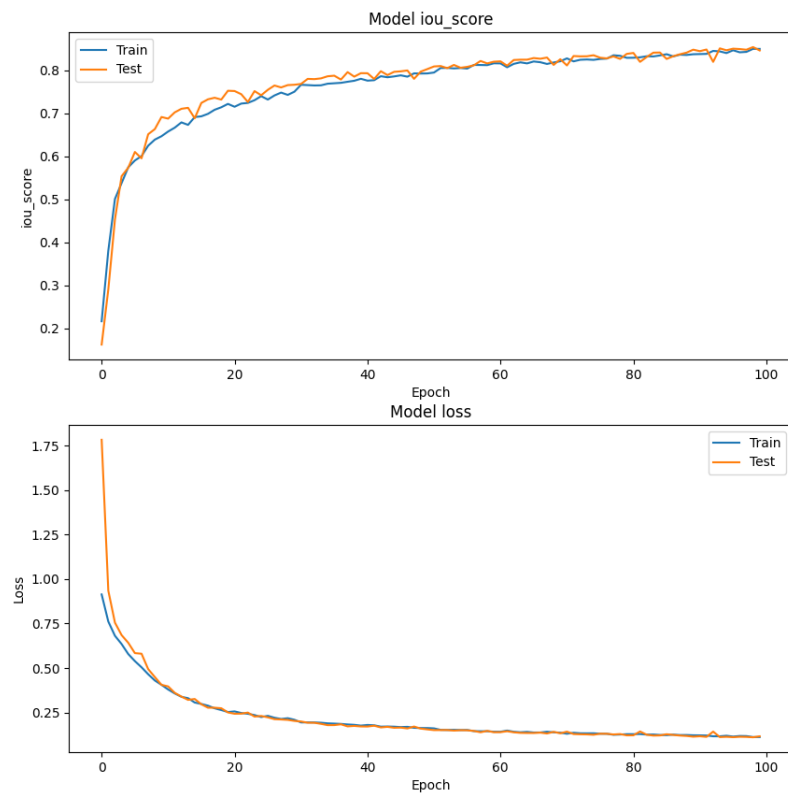


Figure 6: DenseNet121 IoU and Loss values

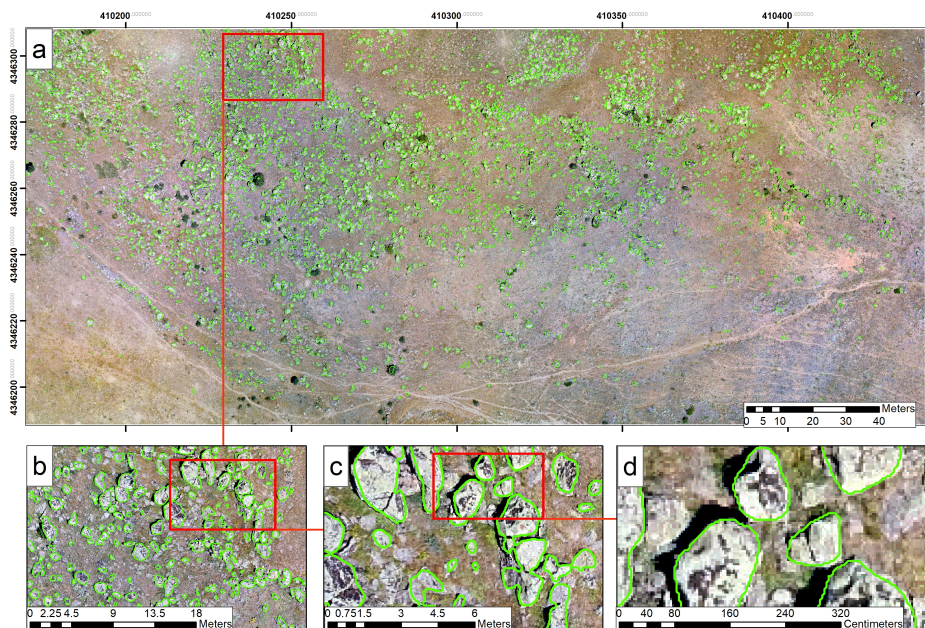


Figure 7: Result map of the model (a) original view, (b,c,d)zoomed views.

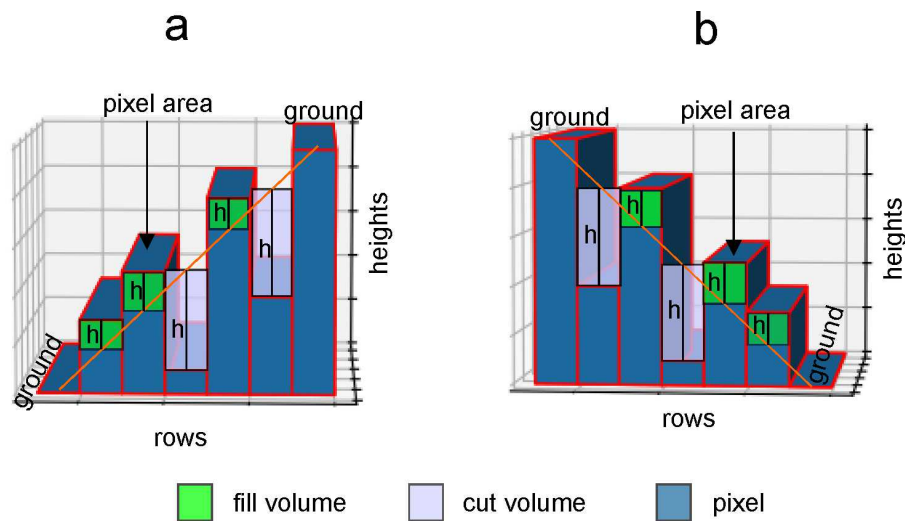


Figure 8: Volume calculation methods. (a) first height is greater than the last height of the rows,(b) b) first height is less than the last height of the rows